Nanoscale Characterization of Interfacial Debonding and Matrix Damage in Titanium Carbide/AA8090 Alloy Particle-Reinforced Metal Matrix Composites

[1]H. B. Nirnajan and A. Chennakesava Reddy[2]

[1]Associate Professor, Department of Mechanical Engineering, M. S. Ramaiah Institute of Technology, Bangalore, India.
[2]Associate Professor, Department of Mechanical Engineering, Vasavi College of Engineering, Hyderabad, India
dr_acreddy@yahoo.com

Abstract: *A hexagonal array unit cell/rhombus TIC nanoparticle RVE models were used to assess micromechanical behavior and interfacial debonding in AA8090/*TiC *composites. The AA8090/TiC metal matrix composites were fabricated at 10%, 20% and 30% volume fractions of TiC. The microstructure of AA8090 alloy/TiC reveals the presence of porosity, interfacial debonding and matrix damage.*

Keywords: AA8090*, titanium carbide, rhombus nanoparticle, RVE model, finite element analysis, debonding, matrix damage.*

1. INTRODUCTION

A key role of the microstructure is most evident in metal matrix composites characterized by distinct internal interfaces. Particle-reinforced metal matrix composites (PRCs) are an important class of composite materials. Due to high elastic moduli, strength, fatigue and wear resistance, these lightweight materials have a number of advantages over ordinary aluminum alloys [1]. Many factors responsible for the macroscopic properties of the composites are discussed in the literature, including load transfer between the matrix and reinforcements, presence of precipitations at the matrix/particle interface, mechanical characteristics of individual components of the materials [2]. An increase in the particle volume content enhances the composite strength and drastically decreases the fracture toughness [3]. Moreover, the irregular shape of reinforcements can significantly affect the cracking process [4]. The presence of coral-shaped Si particles in Al/Si alloys influences the crack evolution pattern in these materials. Similar conclusions are for sharp-cornered particles [5]. In a series of research, a variety of nanoparticle shapes such as spherical [6, 7], ellipsoidal [8-12], rectangular [13], hexagonal [14-16] and rhombus [17] at 10%, 20% and 30% volume fractions were studied and the results computed from a unit cell with uniformly distributed particles were compared.

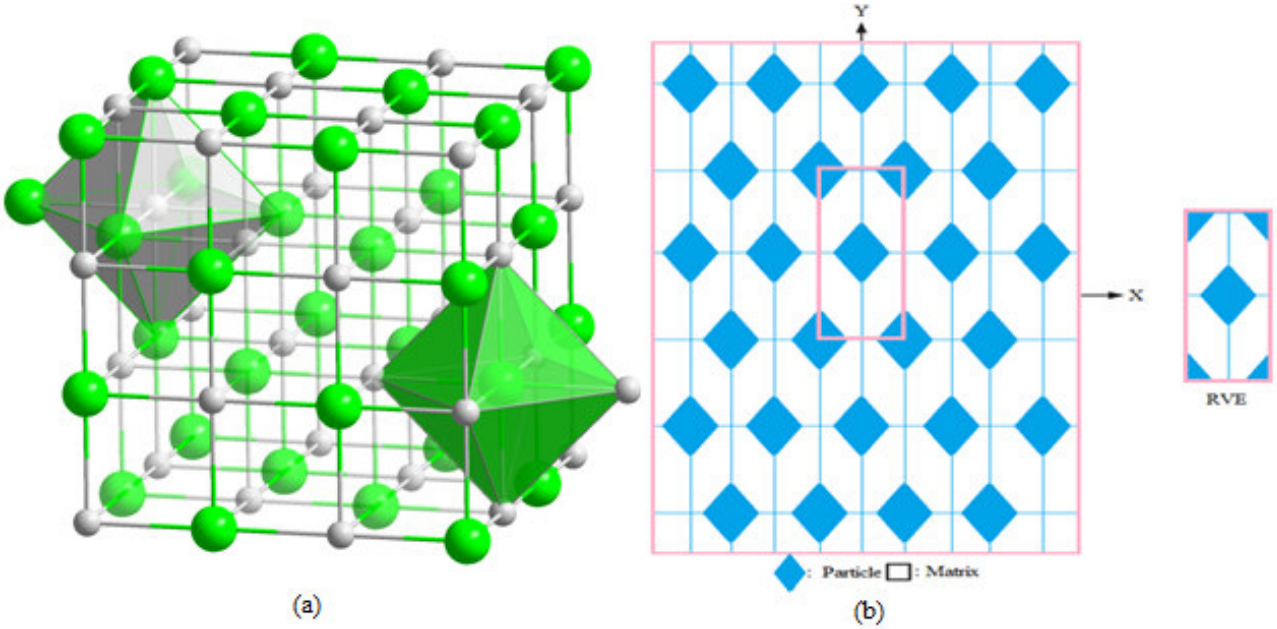

Figure 1: A hexagonal RVE containing a rhombus nanoparticle.

High particle hardness and slick surfaces make titanium carbide (TiC) an ideal filler material tailored to enhance wear-resistant, tribological, and mechanical bearing characteristics. In the present work, titanium carbide nanoparticles were reinforced in AA8090 alloy through the stir casting process. The effect of varying volume fractions of TiC on the microstructural and mechanical properties of AA8090 alloy is investigated. The shape TiC nanoparticle considered in this work is rhombus. The periodic particle distribution was a hexagonal array as shown in figure 1.

2. THEORETICAL BACKGROUND

The strains along x- and y-directions can be determined as using the following equations:

$$\varepsilon_y = -\left(\frac{v_{xy}}{E_x} + \frac{1}{E_z}\right)P = \frac{\Delta y}{a} \quad (1)$$

$$\varepsilon_x = \left(\frac{1}{E_x} - \frac{1}{E_z}\right)P = \frac{\Delta x}{a} \quad (2)$$

The effective elastic moduli and Poisson's ratio in the transverse direction (xy-plane) as follows:

$$E_x = \frac{1}{\frac{\Delta x}{Pa}+\frac{1}{E_z}} \text{ and } E_y = \frac{1}{\frac{\Delta y}{Pa}+\frac{1}{E_z}} \quad (3)$$

$$v_{xy} = \left(\frac{\Delta y}{Pa} + \frac{1}{E_z}\right)/\left(\frac{\Delta x}{Pa} + \frac{1}{E_z}\right) \quad (4)$$

Once the change in lengths along x- and y- direction (Δx and Δy) are determined for the square RVE from the FEA, E_y and E_x and v_{xy} can be determined from Eqs. (3) and (4), correspondingly. Considering adhesion, formation of precipitates, particle size, agglomeration, voids/porosity, obstacles to the dislocation, and the interfacial reaction of the particle/matrix, the formula for the strength of composite is stated below:

$$\sigma_c = \left[\sigma_m\left\{\frac{1-(v_p+v_v)^{2/3}}{1-1.5(v_p+v_v)}\right\}\right]e^{m_p(v_p+v_v)} + kd_p^{-1/2} \quad (5)$$

$$k = E_m m_m / E_p m_p$$

where, v_v and v_p are the volume fractions of voids/porosity and nanoparticles in the composite respectively, m_p and m_m are the possion's ratios of the nanoparticles and matrix respectively, d_p is the mean nanoparticle size (diameter) and E_m and E_p is elastic moduli of the matrix and the particle respectively. Elastic modulus (Young's modulus) is a measure of the stiffness of a material and is a quantity used to characterize materials. Elastic modulus is the same in all orientations for isotropic materials. Anisotropy can be seen in many composites.

The upper-bound equation is given by

$$\frac{E_c}{E_m} = \left(\frac{1-v_v^{2/3}}{1-v_v^{2/3}+v_v}\right) + \frac{1+(\delta-1)v_p^{2/3}}{1+(\delta-1)(v_p^{2/3}-v_p)} \quad (6)$$

The lower-bound equation is given by

$$\frac{E_c}{E_m} = 1 + \frac{v_p - v_p}{\delta/(\delta-1)-(v_p+v_v)^{1/3}} \quad (7)$$

where, $\delta = E_p/E_m$.

The transverse modulus is given by

$$E_t = \frac{E_m E_p}{E_m + E_p(1-v_p^{2/3})/v_p^{2/3}} + E_m\left(1 - v_p^{2/3} - v_v^{2/3}\right) \quad (8)$$

3. MATERIALS METHODS

The matrix material was AA8090 alloy. The reinforcement material was TiC nanoparticles of average size 100nm. The mechanical properties of materials used in the present work are given in table 1.

Table 1: Mechanical properties of AA8090 matrix and TiC nanoparticles

Property	AA8090	ZrO_2
Density, g/cc	2.54	6.15
Elastic modulus, GPa	77	400
Ultimate tensile strength, MPa	119	440
Poisson's ratio	0.33	0.19

AA8090 alloy/TiC composites were fabricated by the stir casting process and low pressure casting technique with argon gas at 3.0 bar. The composite samples were give solution treatment and cold rolled to the predefined size of tensile specimens. The

heat-treated samples were machined to get flat-rectangular specimens (figure 2) for the tensile tests. The tensile specimens were placed in the grips of a Universal Test Machine (UTM) at a specified grip separation and pulled until failure. The test speed was 2 mm/min. A strain gauge was used to determine elongation.

In this research, a cubical representative volume element (RVE) was implemented to analyze the tensile behavior AA8090/TiC nanoparticle composites at three (10%, 20% and 30%) volume fractions of TiC. The large strain PLANE183 element was used in the matrix in all the models. In order to model the adhesion between the matrix and the particle, a CONTACT 172 element was used.

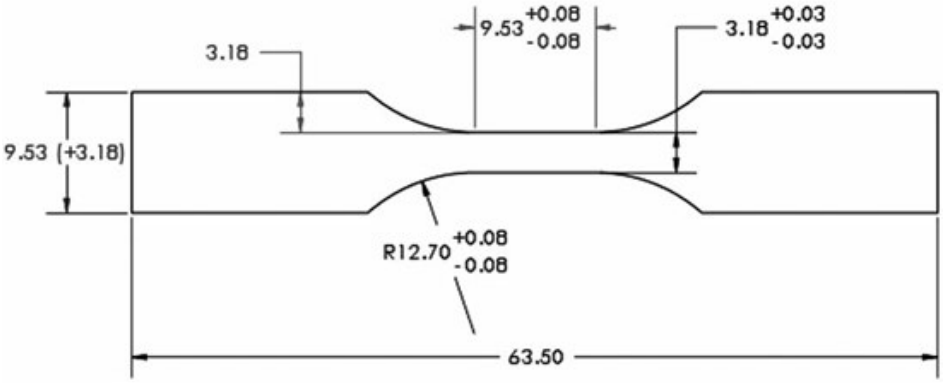

Figure 1: Shape and dimensions of tensile specimen

4. RESULTS AND DISCUSSION

The optical micrograph as shown in figure 3 reveals random distribution of TiC particles in AA8090 alloy matrix. The testes tensile specimens show no necking formation (figure 4). The fracture was at the centre doe a few specimens. The elongation of was decreased with increased volume fraction of TiC particles in AA8090 alloy matrix.

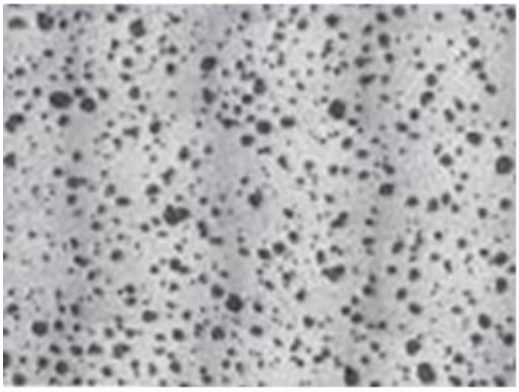

Figure 3: Microstructure showing TIC nanoparticle distribution in AA8090 alloy matrix.

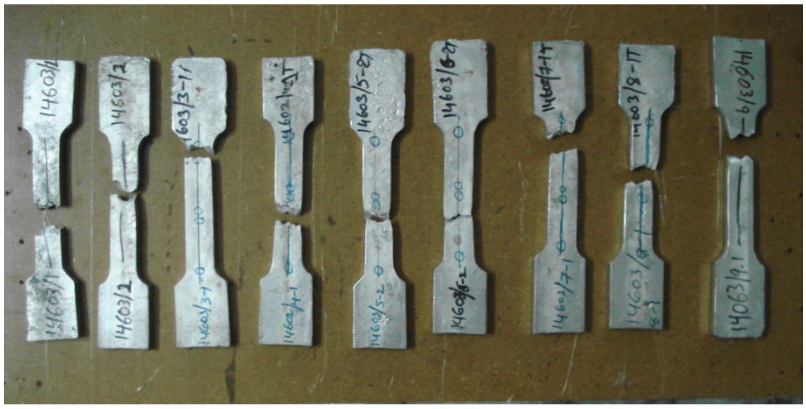

Figure 4: Tested tensile specimens.

3.1 Micromechanical Behavior

Figure 5a represents the normalized tensile strengths of the AA8090 alloy/TiC composites obtained by FEA, present mathematical model, and experimental test. The tensile strength is normalized with ultimate tensile strength of AA8090 alloy. The normalized results obtained from the experimentation and FEA increase with increase of TiC content in the matrix. The difference between the results obtained from experimental procedure and the FEA is due to the ignorance of porosity in the matrix. As seen in figure 5, porosity, interfacial debonding and matrix damage are observed in AA8090/TiC composites. The normalized elastic modulus is shown in figure 4b. The elastic modulus is normalized with the elastic modulus of AA8090 alloy. The stiffness of the composites increases with increase of volume fraction of TiC but the results computed from FEA indicate the loss of stiffness due to increase of TiC particles in the composite. The upper limit (UL) values computed by the present mathematical model are higher than those values obtained by the 'Role of Mixtures (ROM)'and FEA. This is because of assumption of voids in the present mathematical model. The shear strength of the composites decreases with increase of volume fraction of TiC (figure 4c). The major Poisson's ratio increases with increase of volume fraction of TiC particles (figure 4d).

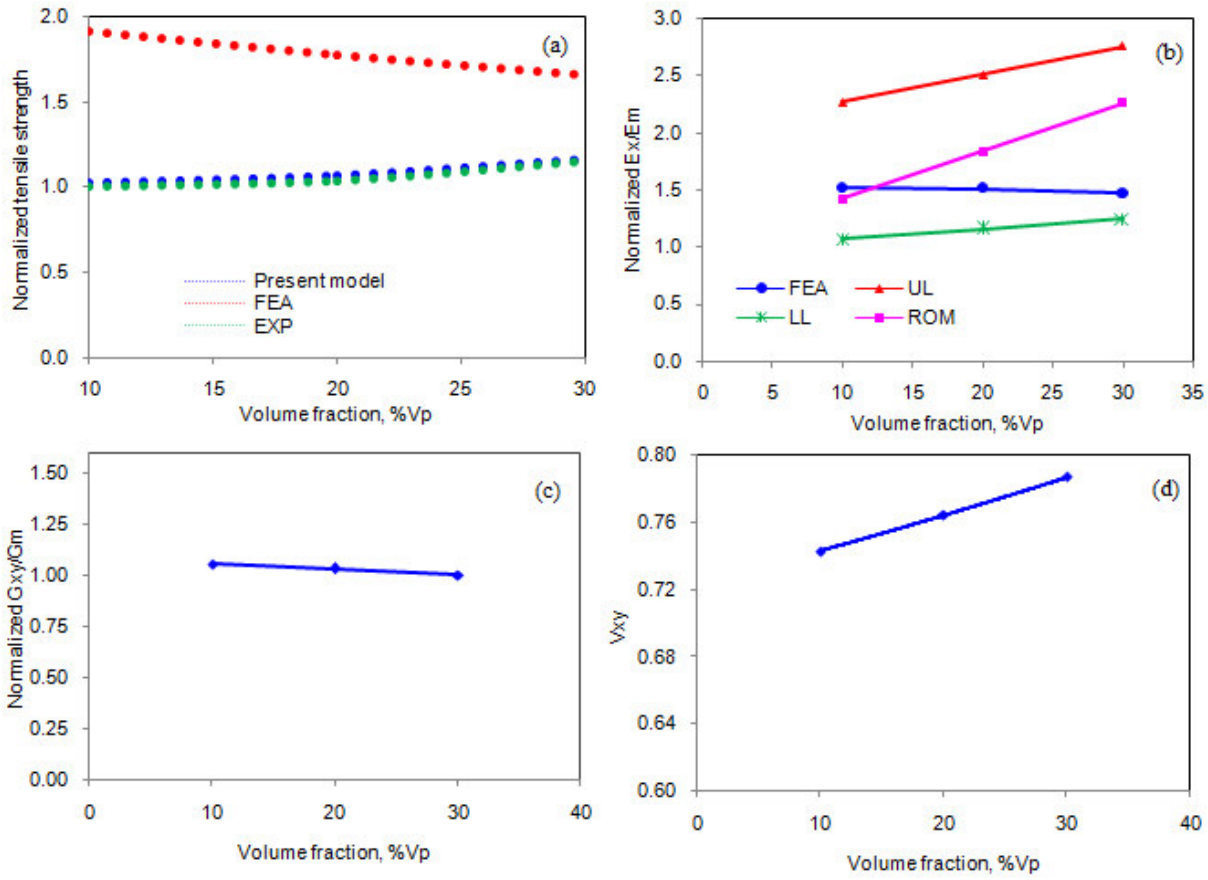

Figure 4: Effect of volume fraction on micromechanical behavior of AA8090/TiC composites.

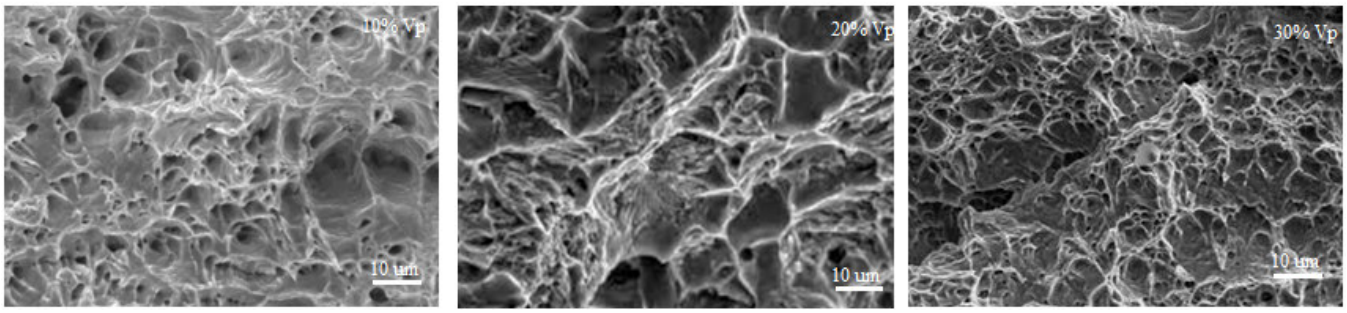

Figure 5: SEM image showing porosity, debonding and matrix damage in AA8090/TiC composites.

3.2 Fracture Analysis

If the particle deforms in an elastic manner (according to Hooke's law) then,

$$\tau = \frac{n}{2}\sigma_p \quad (1)$$

where σ_p is the particle stress. If particle fracture occurs when the stress in the particle reaches its ultimate tensile strength, $\sigma_{p,uts}$, then setting the boundary condition at

$$\sigma_p = \sigma_{p,\,uts} \quad (2)$$

The relationship between the strength of the particle and the interfacial shear stress is such that if

$$\sigma_{P,uts} < \frac{2\tau}{n} \quad (3)$$

Then the particle will fracture. From the figure 6b, it is observed that the TiC nanoparticle was not fractured as the condition in Eq. (11) is not satisfied. For the interfacial debonding/yielding to occur, the interfacial shear stress reaches its shear strength:

$$\tau = \tau_{max} \quad (4)$$

For particle/matrix interfacial debonding can occur if the following condition is satisfied:

$$\tau_{max} < \frac{n\sigma_p}{2} \quad (5)$$

It is observed from figure 6a that the interfacial debonding occurs between TiC nanoparticle and AA8090 alloy matrix as the condition in Eq.(13) is satisfied.

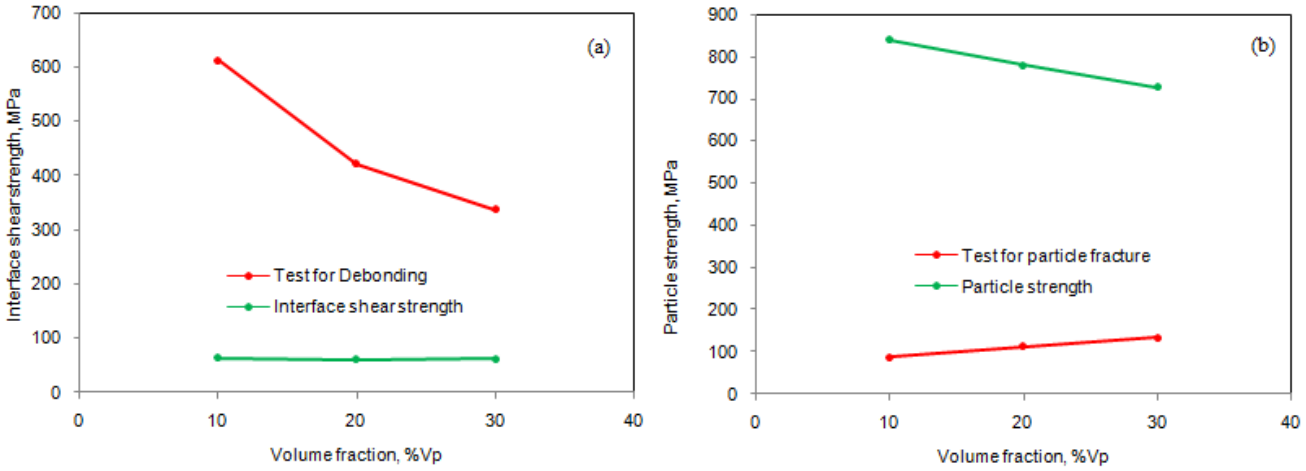

Figure 6: Criterion for interfacial debonding (a) and for particle fracture (b).

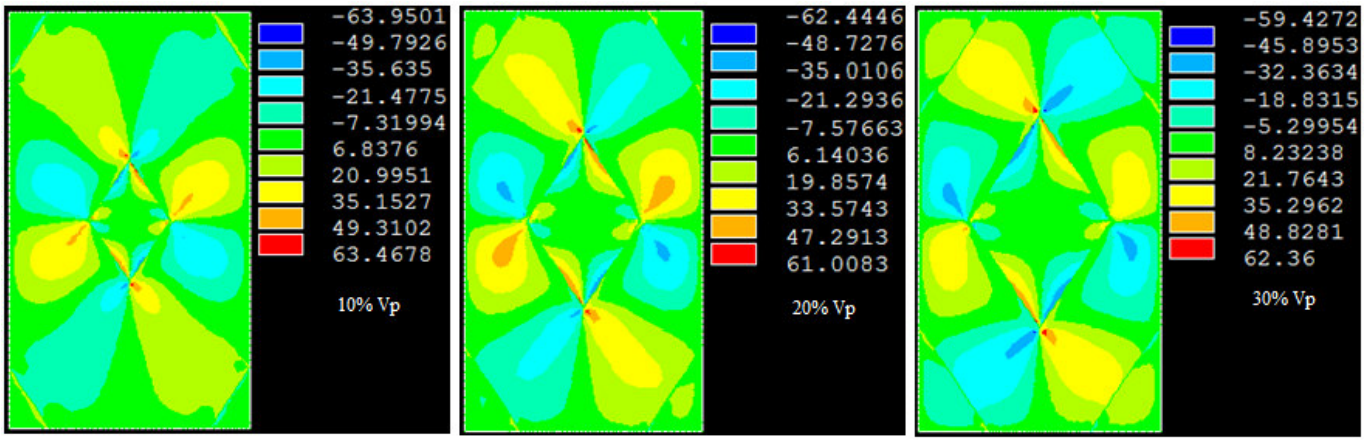

Figure 7: Images of tensile stress obtained from FEA.

As seen from figure 7 the shear stress induced at the interface are higher than that induced in the nanoparticle. Hence, the interfacial debonding was occurred between the particle and the matrix. The matrix fracture is also observed in AA8090/ TiC composites due to inadequate transfer of load from the matrix to the particle.

5. CONCLUSION

The microstructure of AA8090 alloy/TiC reveals the presence of porosity, interfacial debonding and matrix damage in the AA8090 alloy/TiC composites. The shear stress is high at the interface leading to interfacial debonding in AA8090/TiC composites. The matrix damage is also observed in the composites.

REFERENCES

1. M. T. Kiser F. W. Zok, D. S. Wilkinson, Plastic flow and fracture of a particulate metal matrix composite. Acta Materialia, 45, 1996, pp. 3465-3476.
2. D. L. Davidson, Fracture characteristics of Al-4pct Mg mechanically alloyed with SiC, Metallurgical Transactions, 18A, 1991, pp. 2115-2138.
3. T. Christman, A. Needleman, S. Suresh, An experimental and numerical study of deformation in MMCs Acta Metallurgica, 37, 1989, pp. 3029-3050.
4. Q. Shuyi, C. Changrong, Z. Guoding, W. Wenlong, W. Zhongguang, Material Science and Engineering A, 272, 1999, p. 363.
5. M. Lebyodkin, A. Deschamps, Y. Brechet Y, Material Science and Engineering A, 234, 1997, p. 481.
6. A. Chennakesava Reddy, Assessment of Debonding and Particulate Fracture Occurrences in Circular Silicon Nitride Particulate/AA5050 Alloy Metal Matrix Composites , National Conference on Materials and Manufacturing Processes, Hyderabad, India, 27-28 February 1998, pp. 104-109.
7. B. Kotiveera Chari, A. Chennakesava Reddy, Debonding Microprocess and interfacial strength in ZrC Nanoparticle-Filled AA1100 Alloy Matrix Composites using RVE approach, 2nd National Conference on Materials and Manufacturing Processes, Hyderabad, India, 10-11 March 2000, pp. 104-109.
8. A. Chennakesava Reddy, Local Stress Differential for Particulate Fracture in AA2024/Titanium Carbide Nanoparticulate Metal Matrix Composites, National Conference on Materials and Manufacturing Processes, Hyderabad, India, 27-28 February 1998, pp. 127-131.
9. A. Chennakesava Reddy, Micromechanical Modelling of Interfacial Debonding in AA1100/Graphite Nanoparticulate Reinforced Metal Matrix Composites, 2nd International Conference on Composite Materials and Characterization, Nagpur, India, 9-10 April 1999, pp. 249-253.
10. A. Chennakesava Reddy, Micromechanical and fracture behaviors of Ellipsoidal Graphite Reinforced AA2024 Alloy Matrix Composites, 2nd National Conference on Materials and Manufacturing Processes, Hyderabad, India, 10-11 March 2000, pp. 96-103.
11. S. Sundara Rajan, A. Chennakesava Reddy, Micromechanical Modeling of Interfacial Debonding in Silicon Dioxide/AA3003 Alloy Particle-Reinforced Metal Matrix Composites, 2nd National Conference on Materials and Manufacturing Processes, Hyderabad, India, 10-11 March 2000, pp. 110-115.
12. S. Sundara Rajan, A. Chennakesava Reddy, Role of Volume Fraction of Reinforcement on Interfacial Debonding and Matrix Fracture in Titanium Carbide/AA4015 Alloy Particle-Reinforced Metal Matrix Composites, 2nd National Conference on Materials and Manufacturing Processes, Hyderabad, India, 10-11 March 2000, 116-120.
13. A. Chennakesava Reddy, Cohesive Zone Finite Element Analysis to Envisage Interface Debonding in AA7020/Titanium Oxide Nanoparticulate Metal Matrix Composites, 2nd International Conference on Composite Materials and Characterization, Nagpur, India, 9-10 April 1999, pp. 204-209.
14. A. Chennakesava Reddy, Constitutive Behavior of AA5050/MgO Metal Matrix Composites with Interface Debonding: the Finite Element Method for Uniaxial Tension, 2nd National Conference on Materials and Manufacturing Processes, Hyderabad, India, 10-11 March 2000, pp. 121-127.
15. B. Kotiveera Chari, A. Chennakesava Reddy, Interfacial Debonding of Boron Nitride Nanoparticle Reinforced 6061 Aluminum Alloy Matrix Composites, 2nd National Conference on Materials and Manufacturing Processes, Hyderabad, India, 10-11 March 2000, pp. 128-133.
16. P. M. Jebaraj, A. Chennakesava Reddy, Simulation and Microstructural Characterization of Zirconia/AA7020 Alloy Particle-Reinforced Metal Matrix Composites, 2nd National Conference on Materials and Manufacturing Processes, Hyderabad, India, 10-11 March 2000, pp. 134-140.
17. P. M. Jebaraj, A. Chennakesava Reddy, Continuum Micromechanical modeling for Interfacial Debonding of TiN/AA8090 Alloy Particulate Composites, 2nd National Conference on Materials and Manufacturing Processes, Hyderabad, India, 10-11 March 2000, pp. 141-145.